Article

Graphene Supported Tungsten Carbide as Catalyst for Electrochemical Reduction of CO_2

Version June 10, 2019, submitted to Catalysts

Abstract: Electrochemical reduction of CO_2 to useful chemical and fuels in an energy efficient way is currently an expensive and inefficient process. Recently, low-cost transition metal-carbides (TMCs) are proven to exhibit similar electronic structure similarities to Platinum-Group-Metal (PGM) catalysts and hence can be good substitutes for some important reduction reactions. In this work, we test graphene-supported WC (Tungsten Carbide) nanocluster as an electrocatalyst for the CO_2 reduction reaction. Specifically, we perform DFT studies to understand various possible reaction mechanisms and determine the lowest thermodynamic energy landscape of CO_2 reduction to various products such as CO, HCOOH, CH_3OH, and CH_4. This in-depth study of reaction energetics could lead to improvements and develop more efficient electrocatalysts for CO_2 reduction.

1. Introduction

Carbon dioxide (CO_2) is very stable under environmental conditions, and reduction to some hydrocarbon products is an endothermic (or endergonic) process. The process requires a moderate to highly negative potential combined with excellent catalyst kinetic barrier efficiency to minimize the combined energy barriers for this reduction reaction. Several electrocatalysts are being studied to convert CO_2 to useful chemicals and fuels, but they are either limited by high overpotentials or poor product selectivity. In 1985, Hori et al. reported that Cu is a unique metal catalyst which can reduce CO_2 to hydrocarbons efficiently and further studies described that Cu catalyst could electrochemically reduce CO_2 to 16 different products among which CH_4 and C_2H_4 showed higher current densities but at larger overpotentials of up to 1V [1–3]. To overcome this obstacle and make the CO_2 reduction reaction more viable, we require more complex and tailored materials than simple pure transition metals.

Recently, low-cost transition metal-carbides (TMCs) are receiving special attention as electrocatalysts as they have shown improved catalyst stability, activity and selectivity when compared to their parent metal/elements [4,5]. Formation of carbides (with C in the crystal lattice or nanoparticle surface) modifies the metal-atom bonding, increasing the metal-metal distance, thereby causing a contraction in the metal atoms' *d-band*. These d-band contractions would give a better density of states near the Fermi level than their parent metal. In particular, non-noble metal-carbides such as Mo and W display similar electronic structure of noble metals due to their metal-covalent binding and hence can be significant substitutes for precious catalysts in various important catalytic reactions [5]. Additional to electronic and magnetic properties similar to transition metals, they exhibit high melting points like in ionic compounds and hardness similar to covalent solids. Therefore, the bonding in TMCs can be explained as a combination of metallic, covalent, and ionic components [6].

Theoretical and experimental studies proved that TMCs show better catalyst activity in "hydrogen-participating" reactions [7]. For example, metal terminated WC exhibited good activity for hydrogen evolution reaction (HER) and WC coated with Fe when tested for CO_2 reduction are selective towards methane formation. This is because electronic properties of W atoms surrounding Fe are modified, thereby modifying the selectivity. Another interesting phenomenon of TMCs is, they do not follow scaling relations that correlate binding energies of intermediates in a reaction network like other transition metals mainly because of their oxygen affinity i.e., their tendency to bind carbon-bound species weakly compared to oxygen-bound species. This will open up several possibilities to improve their

catalyst activity, selectivity compared to metal catalysts [8,9]. In the same way, in the DFT study of Fe and Co carbides for Fischer-Tropsch synthesis, it is found that FeC (iron carbide) is more active than pure Fe for CO hydrogenation and methane selectivity is higher on Co carbide compared to pure Co [10]. Among different metal-carbides, tungsten carbide (WC) based compounds are widely studied electrocatalysts [11] . They are investigated in various forms, such as:

1. alloys to combine the electronic properties of WC with other metal(s) for example Tantalum doped WC displayed better activity towards hydrogen evolution (HER) when compared to unmodified WC [12].
2. specific shape and structural arrangement like core-shell structures of WC with monolayer metal coatings are stable against CO poisoning thereby improving the activity of methanol electrooxidation [13–16] .
3. catalyst support to increase the electrocatalytic activity leading to better performance of the fuel cells such as WC supported Pt is found to be more thermally and electrochemically stable than Pt/C for oxygen reduction reaction [17,18] .
4. co-catalyst to the catalytic system where strong electronic interactions between them might modify (maximize) the electrocatalytic activity. As an example, Ni with WC nanocluster for urea electro-oxidation showed high tolerance towards CO poisoning, and high stability thereby enhancing catalyst activity [19].

All these studies explain that TMCs have the potential to work as better catalysts making them an attractive alternative for traditional metallic catalysts in some of the industrially relevant catalytic reactions. Nanocatalysts in the form of nanoclusters where the atoms are structurally quasi-defined to well-defined help in experimental and theoretical investigations of important electronic structure properties in CO_2 electroreduction reaction (CO_2RR). Additionally, graphene as a catalyst support further improves the active surface area for the catalyst systems by providing minimal adsorption footprint for the TMC NP. Other unique properties of this two-dimensional structure such as high stability and electrical conductivity – which can modify the TMC NP electronic structure- help in selectivity and cost reduction of catalysts playing a pivotal role in most of the heterogeneous catalyst systems [20].

Motivated by all the above aspects, in this study we ***test graphene supported WC nanocluster as an electrocatalyst for CO_2RR.*** This work determines the performance of WC/graphene as a catalyst system for CO_2 reduction to various products such as CO, HCOOH, CH_3OH, and CH_4 which possibly could be the platform for designing new and improved TMC electrocatalysts for this important reduction reaction. To achieve this, we have calculated binding free energies of all possible reaction intermediates and analyzed the reaction mechanisms in detail by focusing on understanding the effect solvation energies on product selectivity and catalyst activity and lastly determined the lowest energy pathways for all the products mentioned above. We inferred that CH_4 is favored over CH_3OH on WC/graphene at lower reducing potentials. From literature, CH_3OH formation is less preferred on WC and metal-coated WC because of the stronger binding of O* and OH* bound species [16,21,22] Results from current work explain that the reduction to CH_3OH on graphene supported WC is thermodynamically favorable at higher negative potentials compared to reduction to CH_4 which is in qualitative agreement with the results from the literature.

2. (Computational) Materials and Methods

We use Density functional theory (DFT) to understand catalyst surface reaction pathways in detail. We perform plane wave DFT calculations with VASP (Vienna Ab Initio Simulation Package) to find optimized surface structures and calculate electronic structure properties such as ground state energies, binding energies, charge densities, and perform bader charge analysis [23–28] . Throughout this work, all the electronic structure calculations are performed using the Van Der Waals, opt-PBE functional as they are proven to show high accuracy to study adsorption properties [29–31]. A Fermi smearing of 0.2 eV is used and calculations are performed with gamma centered *k*-points mesh of 2x2x1 with a convergence of ground state energies up to 10^{-5} eV/mole-unit cell with respect to *k*-point sampling [32] . A vacuum space of 12 Å is defined to minimize the interactions between repeated structures in the direction parallel to the surface normal of the graphene plane. All the reaction energy calculations are completed using the lowest energy conformation of the intermediate species. Detailed images of the structure and some adsorbate snapshots are provided in the Supporting Information submitted with this manuscript.

We take advantage of computational hydrogen electrode (CHE) approach for screening and designing electrocatalysts primarily to understand reaction mechanisms for CO_2 electroreduction to CH_4 and CH_3OH [33–35]. Possible reaction pathways for electrochemical reduction of CO_2 to CO, CH_4 and CH_3OH are shown in **Figure 1**. We use RHE (reversible hydrogen electrode) as the reference electrode throughout this work. Since the RHE is the reference for all the reactions, it can be set to zero. The overall reactions for CO_2 reduction to products and their corresponding thermodynamic equilibrium potentials are shown in **Table 1** below.

Table 1. Overall reactions for CO2 reduction to different products and their equilibrium potentials (U, V vs. RHE) [36]

Reaction	U (V vs. RHE)
$CO2 + 2\,(H^+ + e^-) \rightarrow CO + H2O$	-0.10
$CO2 + 2\,(H^+ + e^-) \rightarrow HCOOH$	-0.20
$CO2 + 6\,(H^+ + e^-) \rightarrow CH3OH + H2O$	-0.03
$CO2 + 8\,(H^+ + e^-) \rightarrow CH4 + H2O$	0.17

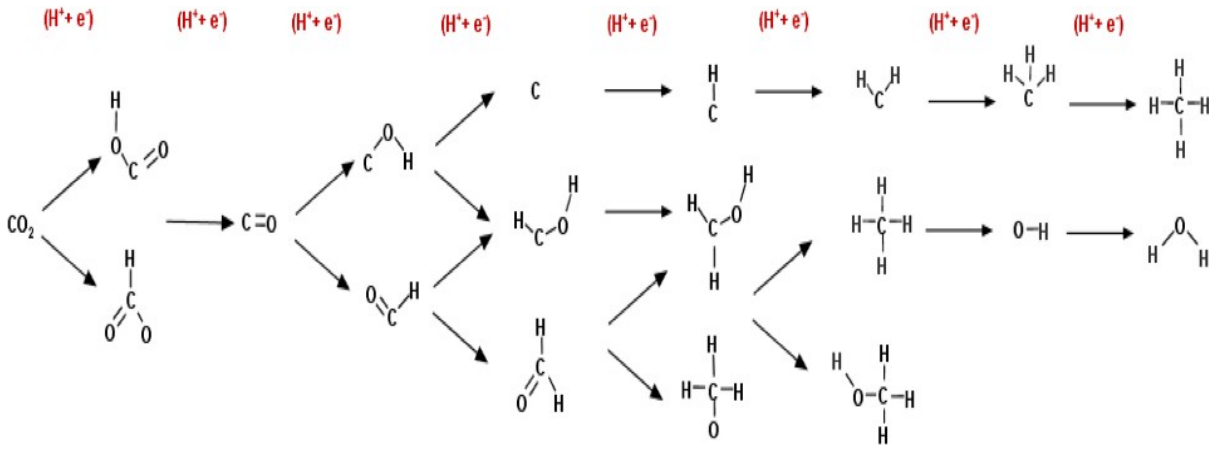

Figure 1. Possible reaction energy mechanisms for electrochemical reduction of CO2 to CO, CH4, and CH3OH. OH, and H2O formed along the reaction pathways are omitted in the figure for clarity.

The Binding energy of each intermediate species in the reaction network can be calculated using equation (1). This is the difference between DFT energy of adsorbed intermediate species and sum of DFT energy of bare surface and formation energies of C, H, O w.r.t gaseous DFT energies of CO, H_2, and H_2O.

$$\Delta E_{binding} = E_{DFT} - (E_{surface} + x E_C + y E_H + z E_O) \quad (1)$$

Similarly, the free energy of each electrochemical step in the reaction pathway corrected by zero-point energies (ZPE) with enthalpy and entropy contributions at potentials other than 0V can be estimated using equation (2) given below.

$$\Delta G(U) = \Delta E_{rxn} + \Delta ZPE + \int C_p\, dT - T\Delta S - neU \quad (2)$$

U is the applied potential to make the elementary step exergonic (known as limiting potential, U_L) and n is the number of proton-electron pairs consumed in each step. The ZPE, enthalpy, and entropy of adsorbed species are obtained from previously determined values as they are assumed to be largely indepdent of catalyst surface and therefore can be approximated to be the same for all structures [33,37]. Since an explicit treatment of a number of water molecules is tedious to carry out using DFT methods, we have used implicit method in VASP with the default dielectric constant of H_2O to calculate solvation energies. These are generally much less computationally demanding than explicit methods but can reproduce significant results like explicit methods for O*, OH* bound intermediate species [38,39] .

3. Results and Discussion

We study several possible reaction intermediates and plot free energy diagrams for various possible reaction mechanisms to determine the lowest energy pathway for each product. As we apply higher (larger magnitude) negative voltages to different reaction pathways, the pathway with the smallest positive rate-limiting step will be the first pathway to become entirely exergonic across all steps in the pathway. This pathway will be the best lowest energy reaction pathway for CO_2RR. These FEDs provide an overall understanding of the reaction mechanism, electrocatalytic activity for CO_2RR as well as selectivity of products. Here, we focus on the lowest ΔG pathway for CO_2RR to CO, HCOOH, CH_3OH, and CH_4.

CO and HCOOH as products:

Figure 2 and **Figure 3** show the lowest energy pathway for CO_2 reduction to HCOOH and CO at 0V vs. RHE on graphene supported WC. These products are obtained by two proton-electron transfers along the reaction pathway. CO_2 is first protonated to form either COOH* or OCHO*. The limiting potential for HCOOH and CO formation depends on how strongly or weakly COOH* and OCHO* bind to the surface. When we compare binding free energies, the formation of COOH* is less exergonic compared to OCHO*. A second proton-electron transfer results in the formation of HCOOH and CO. Although OCHO* is more stable compared to COOH*, the pathway via COOH* will minimize the rate limiting step by around 1.9V for HCOOH formation and 2.5V for CO formation. This larger difference in binding free energies of COOH* and OCHO* is due to the fact that COOH tries to bind to the surface of the catalyst via C and O atom and OCHO binds to the surface of the catalyst via two oxygen atoms and WC has strong oxygen affinity i.e., it binds O* and OH* bound intermediate species very strong, creating huge energy barriers.

Figure 2 shows the lowest energy pathway for HCOOH formation. The calculated limiting potential for HCOOH formation is -2.45V and the potential determining step, i.e. the rate-limiting step is the formation of HCOOH from COOH*. **Figure 3** shows the lowest energy pathway for CO formation. The calculated limiting potential for CO formation is -1.36V and the rate-limiting step is the formation of CO from COOH*. This is in agreement with previous experimental and theoretical studies showing the reduction potential for CO_2 to CO is in the range of -0.72V to -1.5V on pure metal surfaces such as Ag, Au, Zn. This comparison also confirms that WC/graphene can be used as an alternative for precious electrocatalysts for CO_2 reduction to CO. Further reduction of CO* to CH_3OH and CH_4 as products is determined by the binding energy of CO*. Stronger binding of CO* results in hydrogen evolution due to CO poisoning and weaker binding of CO* results in CO desorption before further reduction to products. It is proven from previous work that metals such as Ag, Au, and Zn that bind CO weakly during CO_2 reduction can further reduce to CH_3OH and CH_4 but at higher negative potentials. Therefore, in the next section, we will discuss CO_2 reduction to CH_3OH and CH_4 on graphene supported WC.

CH_3OH and CH_4 as products:

This section discusses the lowest energy pathways for CO_2 reduction to CH_3OH and CH_4 at 0V on graphene supported WC. These products are obtained by six and eight proton-electron transfers, respectively, along the reaction pathway. The first two steps up to CO* formation is very well understood from the previous section. However, complexity arises when CO* is further protonated. As the number of protons-electrons transferred increase, the number of required intermediates in each reaction network increases. This is one of the reasons why CO_2 electrochemical reduction reaction mechanism and its thermodynamics is more complex to study when compared to oxygen reduction reaction (ORR), hydrogen evolution reaction (HER) and other reactions involving the transfer of fewer proton-electron pairs. Similar to CO and HCOOH formation, CH_3OH and CH_4 product formation follow a reaction pathway via COOH*. The protonation of CO* in electrochemical reduction to CH_3OH and CH_4 can follow either oxophilic pathway (CO* is protonated at C atom to form HCO* and bind to the surface of the catalyst via O atom) or carbophilic pathway (CO* is protonated at O atom to form COH* and binds to the surface of the catalyst via C atom).

<u>CH_3OH as a product:</u>

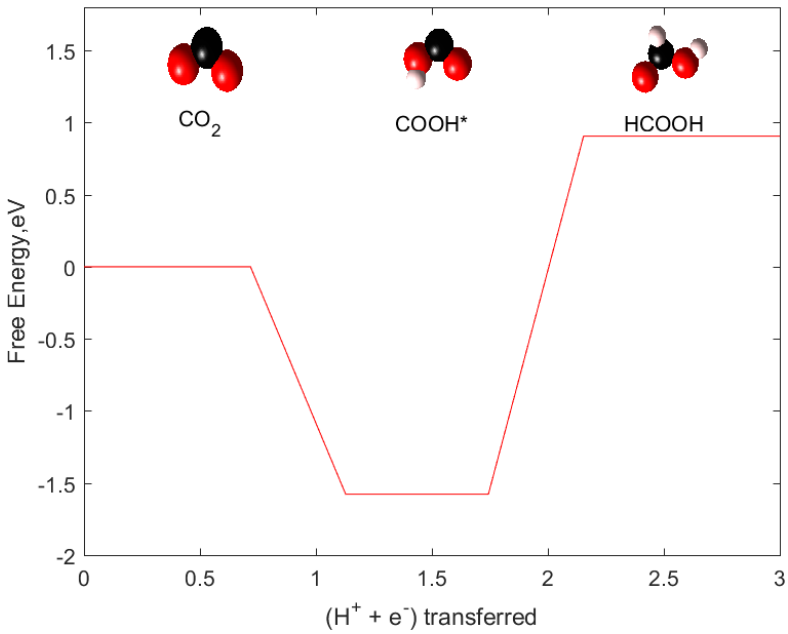

Figure 2. Lowest energy pathway of CO_2 reduction to HCOOH at U=0V on WC/graphene. Color code of atoms: red: oxygen, black: carbon, white: hydrogen

Figure 3. Lowest energy pathway of CO_2 reduction to CO at U=0V on WC/graphene. Color code of

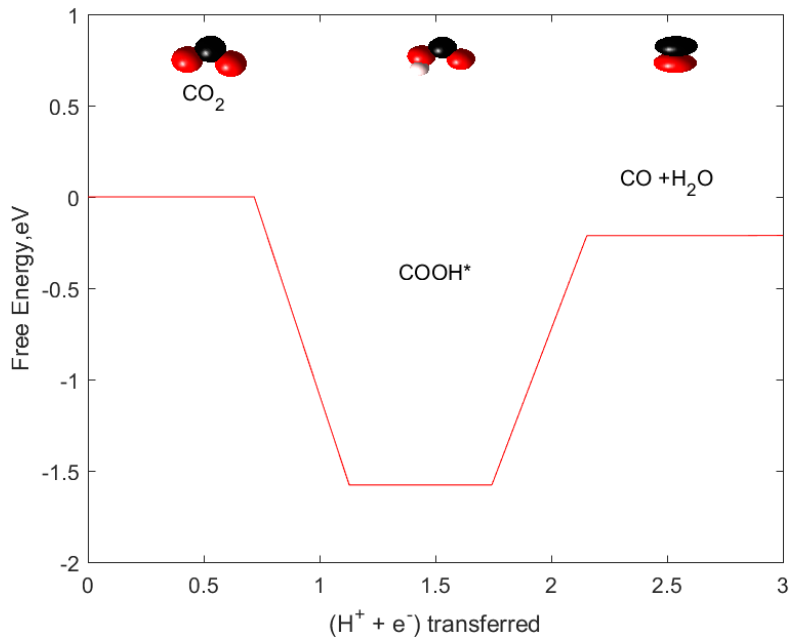

atoms: red: oxygen, black: carbon, white: hydrogen

Figure 4 and **Figure 5** display the lowest energy pathway for CH_3OH formation with and without taking solvation energies into account. Apart from the reaction mechanism, these free energy diagrams also guide us in understanding the effect of solvation on the reaction thermodynamics in CH_3OH formation. In **Figure 4**, we have shown the lowest energy pathway for CH_3OH formation when solvation energies are excluded. Real aqueous phase electrochemical CO_2RR has water molecules present around the TMC NP, and these water molecules can stabilize the reactants, products, and intermediates through H-bonding. The protonation of CO* in this product formation is via oxophilic pathway i.e., via HCO* species. If the solvation effect is not considered, the calculated limiting potential for the product formation is -0.56V with rate-limiting step of CH_3O* to CH_3OH formation. **Figure 5** shows the lowest energy pathway with addition of solvation energies. Inclusion of solvation energies in electrochemical reduction to CH_3OH modified ***not only the reducing***

potential but also the lowest energy reaction pathway and the rate-limiting step. The limiting potential is increased from -0.56V to -1.79V and the reaction pathway is shifted from oxophilic to carbophilic pathway i.e., the pathway is shifted from HCO* to COH*. The new rate-limiting step is the formation of CHOH* from COH*. It is worth noting that, these changes in the reaction pathway, rate-limiting step and its corresponding potential is due to the following reason: WC has strong oxygen affinity; therefore, it strongly binds all O* and OH* bound intermediate species. Inclusion of solvent effect have further stabilized these O*, and OH*bound intermediate species altering the electronic binding free energies thereby creating huge energy barriers in the reaction network.

For additional comparison, in Figure 5 we have included the carbophilic pathway without solvation energies (red pathway). The calculated limiting potential for the product formation is -1.73V with rate-limiting step COH* to CHOH*. Inclusion of solvation energies (blue pathway) has stabilized the adsorbate species and minimized the reducing potential by ~ 0.06V without modifying the rate-limiting step of carbophilic pathway.

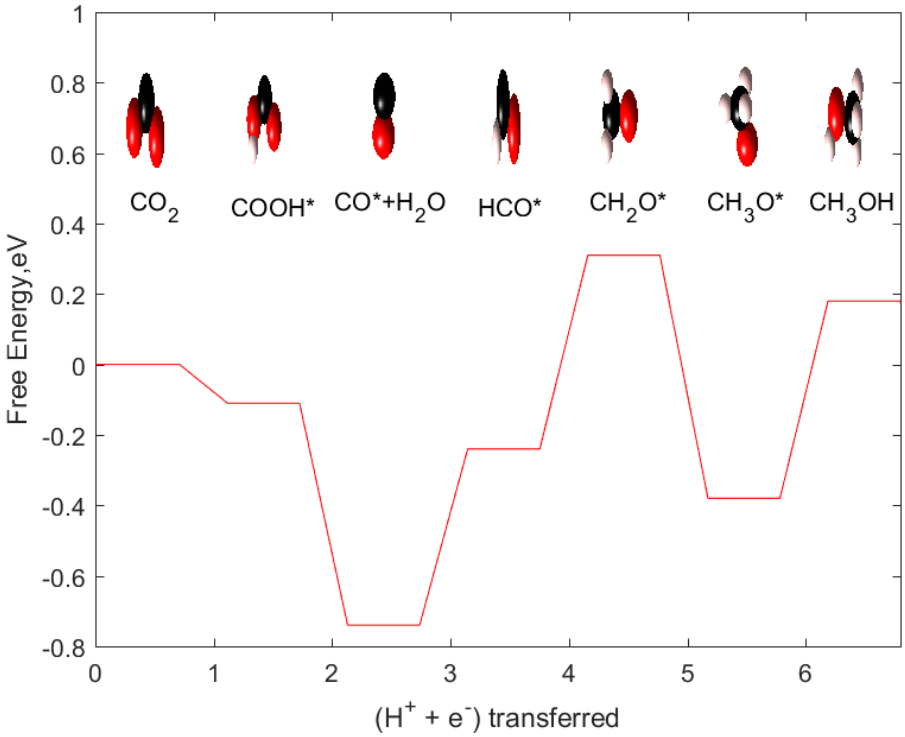

Figure 4. Lowest energy pathway of CO_2 reduction to CH_3OH on the WC/graphene excluding solvation effect. Color code of atoms: red: oxygen, black: carbon, white: hydrogen

CH_4 as a product:

Similarly**, Figure 6 and Figure 8** display the lowest energy pathway for CH_4 formation with and without taking solvation energies into account**. Figure 6**, red pathway shows the lowest energy pathway without solvation energy correct factor and the calculated limiting potential for the product formation is -1.58V with the same rate-limiting step i.e., CO* to COH*. The blue pathway is the lowest energy pathway after adding the solvation correction factor and the calculated limiting potential for product formation is -0.84V, and the rate-limiting step is the formation of CO* from COH*. The key point here is, the inclusion of solvation energies minimized the reducing potential by around 0.75V but did not modify the lowest energy reaction pathway. This may be due to the fact that CH_4 formation pathway is via the carbophilic pathway and carbon bound species. Therefore, the effect of solvation stabilized the COOH*, CO* and COH* binding free energies modifying just the first four steps in the reaction pathway.

Figure 7 and **Figure 8** show calculated lowest energy profiles including solvation energies for a complete series of elementary steps leading to CH_3OH and CH_4 formation, respectively. We have also included the free energy profile of product formation at thermodynamic limiting potential/reducing potential i.e., the potential at which all the elementary steps are downhill (exergonic) in free energy. This is used to determine the overpotentials of the reaction on a particular electrocatalyst. Overpotentials

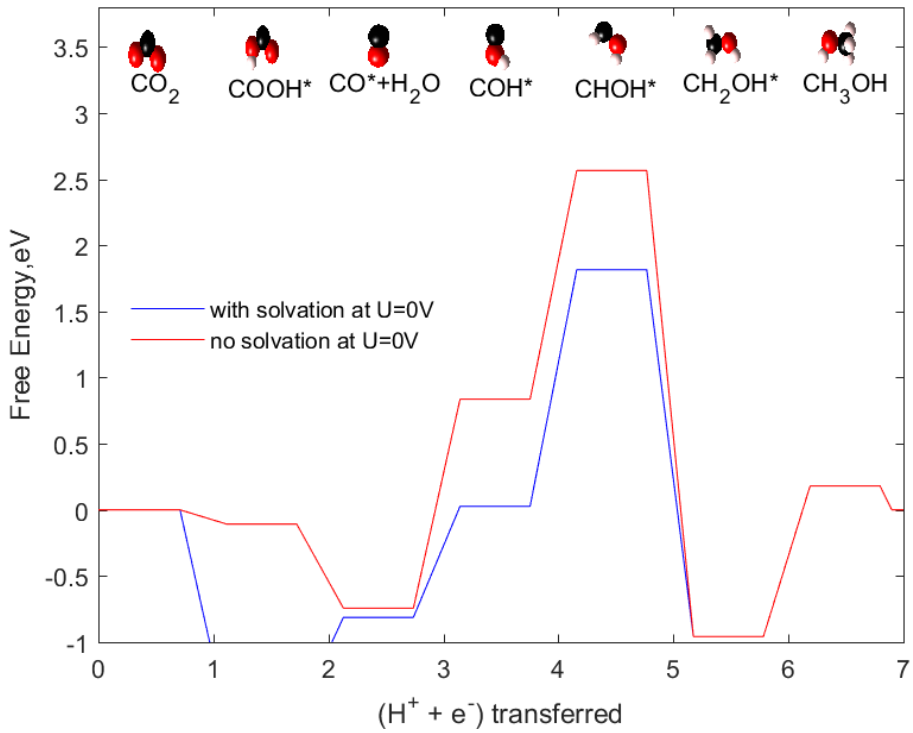

Figure 5. Lowest energy pathways of CO_2 reduction to CH_3OH on the WC/graphene. Blue pathway: including solvation energy correction factor. Red pathway: without solvation energy correction factor. Color code of atoms: red: oxygen, black: carbon, white: hydrogen.

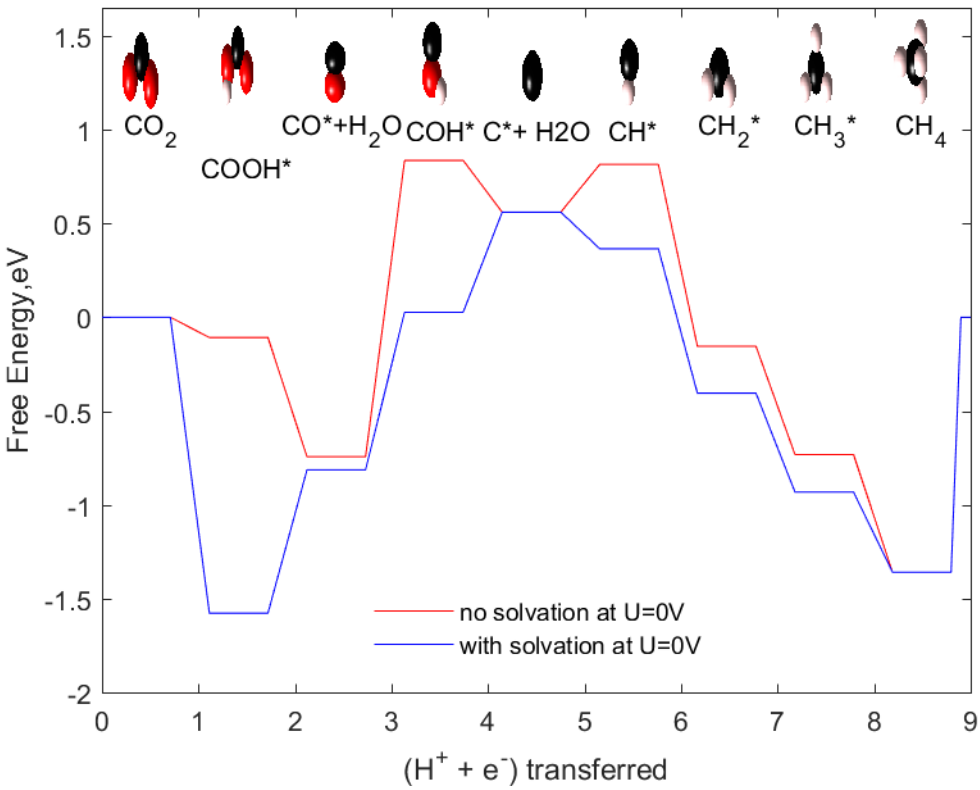

Figure 6. Lowest energy pathway of CO_2 reduction to CH_4 on the WC/graphene. Red: excluding solvation effect. Blue: including solvation effect. Color code of atoms: red: oxygen, black: carbon, white: hydrogen.

can be directly related to the catalyst activity and energy efficiency and can be obtained by the difference between the equilibrium potential and limiting potential. On our catalyst system, CO_2 can reduce to CH_3OH with an overpotential of 1.81V and CH_4 with an overpotential of 0.67V. For additional comparison we have shown free energy profile at the equilibrium potentials, and the maximum potential allowed by the thermodynamics.

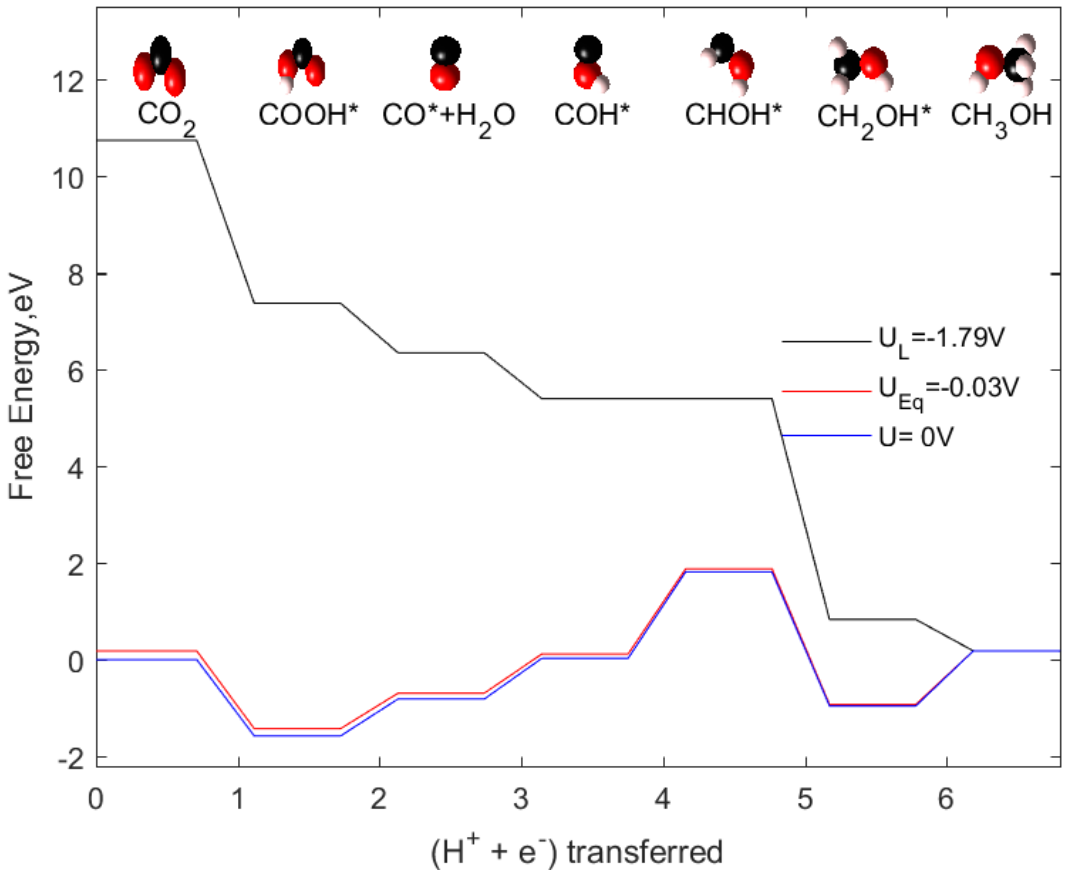

Figure 7. Reaction energy profiles for CO_2 reduction to CH_3OH at 0V vs. RHE (blue), thermodynamic limiting potential of (U_L) -1.79V vs. RHE (black) and equilibrium potential (U_E) of -0.03V vs. RHE (red). Color code of atoms: red: oxygen, black: carbon, white: hydrogen.

Comparison of CO_2 reduction to CH_4 and CH_3OH on graphene supported WC nanocluster and WC (0001):

In this section, we compare CO_2 reduction on WC/ graphene to that on WC (0001). Our analysis and comparison are based on the reaction free energy profile. From the work of Wannakao S et al., the limiting potential for CO_2 reduction to CH_4 on WC (0001) is -0.35V (no solvation) which is 0.5V (with solvation) lower than the potential achieved in current work. Similarly, the limiting potential for CH_3OH formation on WC (0001) is around -0.39V (no solvation) which is around 1.5V (with solvation) lower than the potential achieved in current work. This difference in potential could be due to the following reasons:

1. Employing different functionals in the DFT calculations would result in differences in binding free energies of intermediates. In the work of Wannakao S, et al., it is proven that the binding energies obtained with the PBE functional are 0.2eV higher than those obtained with the RPBE functional.

2. Another reason is predicted to be due to the coverage of adsorbed intermediates on the surface of the catalyst. Our catalyst system is designed by placing only one adsorbate species on single nanocluster which is approximately equal to 1/6 or 1/9 ML coverage of adsorbate species on the surface (assuming each side of the cluster mimics 3 × 2 or 3 × 3 slab surface).

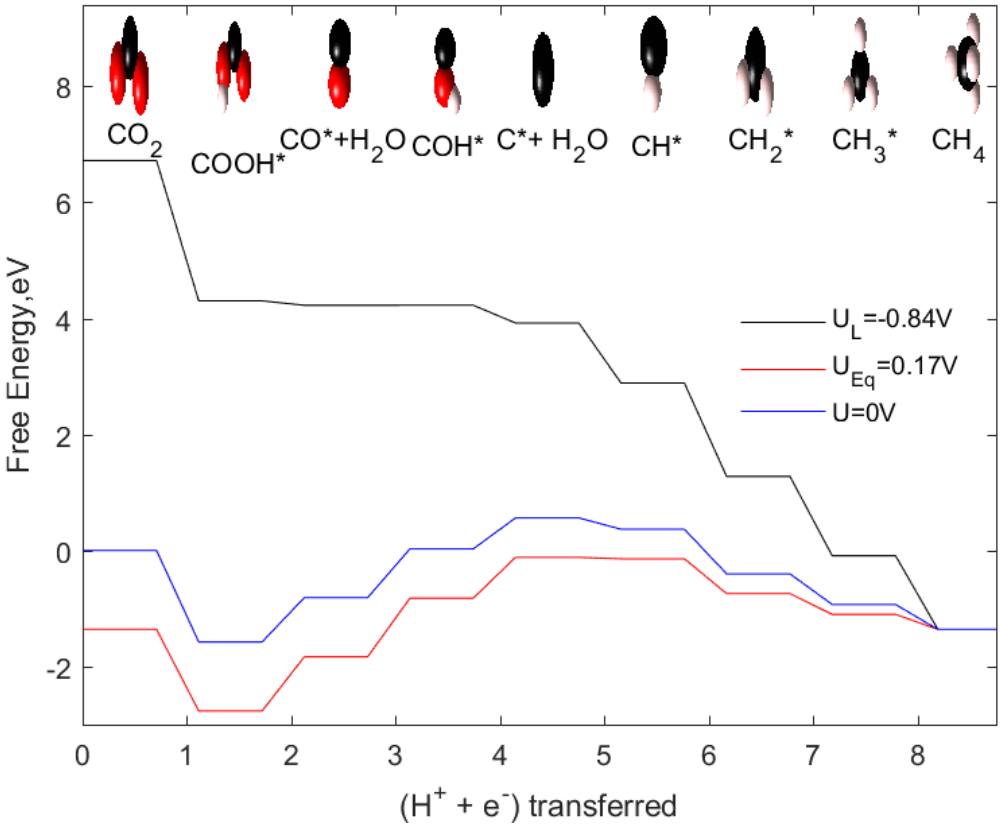

Figure 8. Reaction energy profiles for CO_2 reduction to CH_4 at 0V vs. RHE (blue), thermodynamic limiting potential (U_L) of -0.84V vs. RHE (black) and equilibrium potential (U_E) of 0.17 V vs. RHE (red). Color code of atoms: red: oxygen, black: carbon, white: hydrogen.

However, in the work of Wannakao S, et al., WC (0001) was modeled by 1/6 to 1/9 monolayer coverage of adsorbate species which means these are placed comparatively closer than our adsorbate species arrangement. We predict that the influence of lateral interactions between adsorbed intermediates could also lead to a difference in reaction free energies. To investigate this, we vary (increase) the surface coverage of intermediate species by placing two species instead of one on our catalyst system as neighboring atoms/moieties near the active site. In other words, this system is modified to try to approximate the effects of 1/6 to 1/9 ML coverage of adsorbate species in their work.

Figure 9 shows how the reaction free energies vary when the proportion of adsorbate coverage on the catalyst system varies. Here, we have computed the free energies of initial steps in the reaction network (COOH*, CO*, COH*) as these are the pathway determining intermediates. Co-adsorption of these species generated an upward shift of binding free energies of all the initial three steps. Consequently, the rate-limiting step in the case of co-adsorbed species shifted to COOH* protonation step from CO* protonation step. This analysis also explains that surface coverage of adsorbed species plays equally important role in determining the energetics of CO_2 reduction reaction.

Role of Graphene:

In WC-graphene system, the energy barrier of rate-limiting step is 0.85V whereas the energy barrier of rate-limiting step for WC nanocluster is 1.04V. In other words, CO* and COH* are further stabilized on graphene supported WC. Therefore, graphene as a support for WC catalyst enhances the energy efficiency of CO_2 reduction reaction by lowering the limiting potential by ~0.2V. **Figure 10** compares the free energies of initial steps in the reaction network (COOH*, CO*, COH*) on graphene supported WC and plain WC nanocluster. Therefore, instead of numerical comparison of binding free energies and reduction potentials on graphene supported WC and WC (0001), we have compared the reaction pathways and potential determining steps. We have graphically represented the reaction pathways of CH_4 formation on WC/graphene and WC (0001) in **Figure 11** to show the similarities between them.

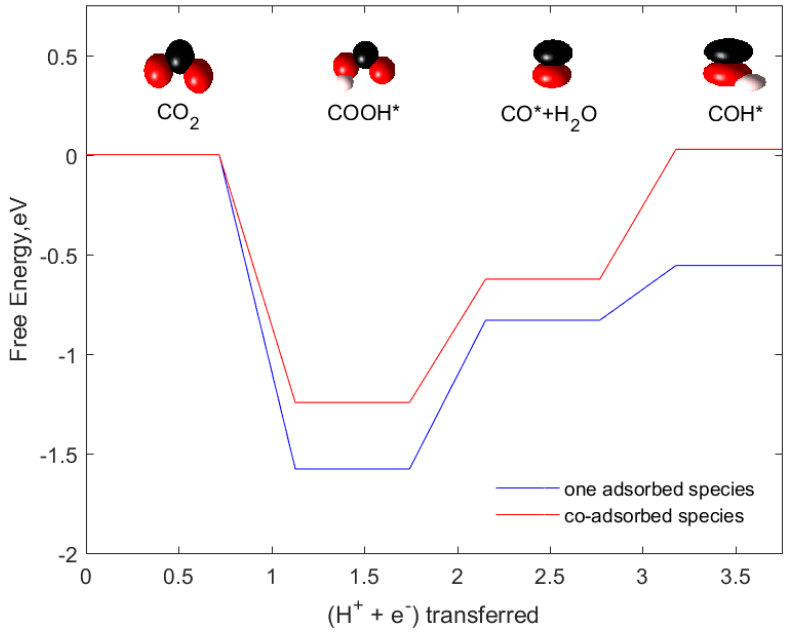

Figure 9. Role of surface coverage on reaction energetics. Blue: one adsorbed species per WC/graphene catalyst system. Red: Co-adsorbed species per WC/graphene catalyst system. Color code of atoms: red: oxygen, black: carbon, white: hydrogen.

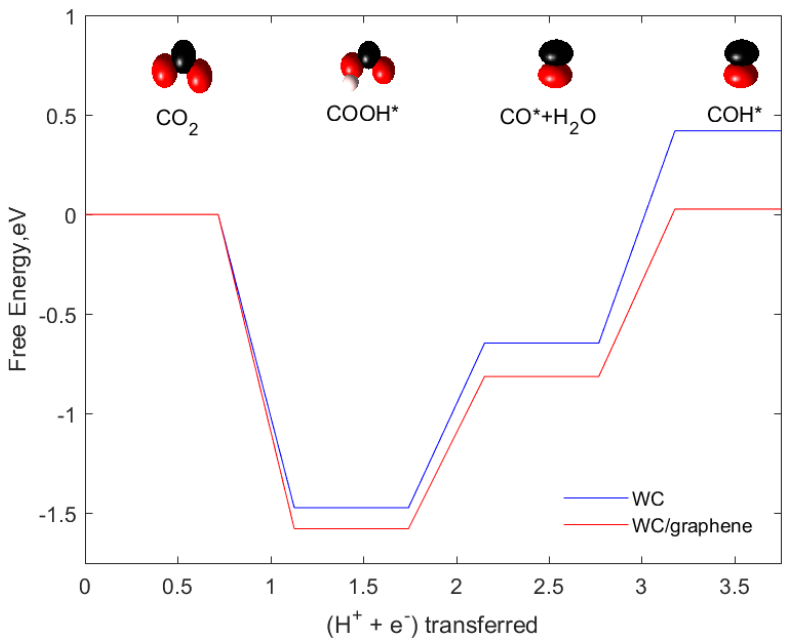

Figure 10. Comparison of reaction energetics of CO_2 reduction on WC nanocluster (blue) and graphene supported WC nanocluster (red). Color code of atoms: red: oxygen, black: carbon, white: hydrogen.

From literature, CH_4 formation on WC (0001) follows a reaction pathway via COOH* and COH* with CO* protonation to COH* as the potential determining step. Similarly, current work shows that the lowest energy pathway for CO_2 reduction follows the carbophilic pathway with identical rate-limiting step and binding site (binds to W through C from COH*). Also, while comparing COH* and HCO* binding energies, both on WC/graphene and WC (0001), HCO* (via C and O atoms) binds more strongly than COH* (via C atom) and in both the cases pathway via COH* minimizes the reducing potential when compared to HCO*.

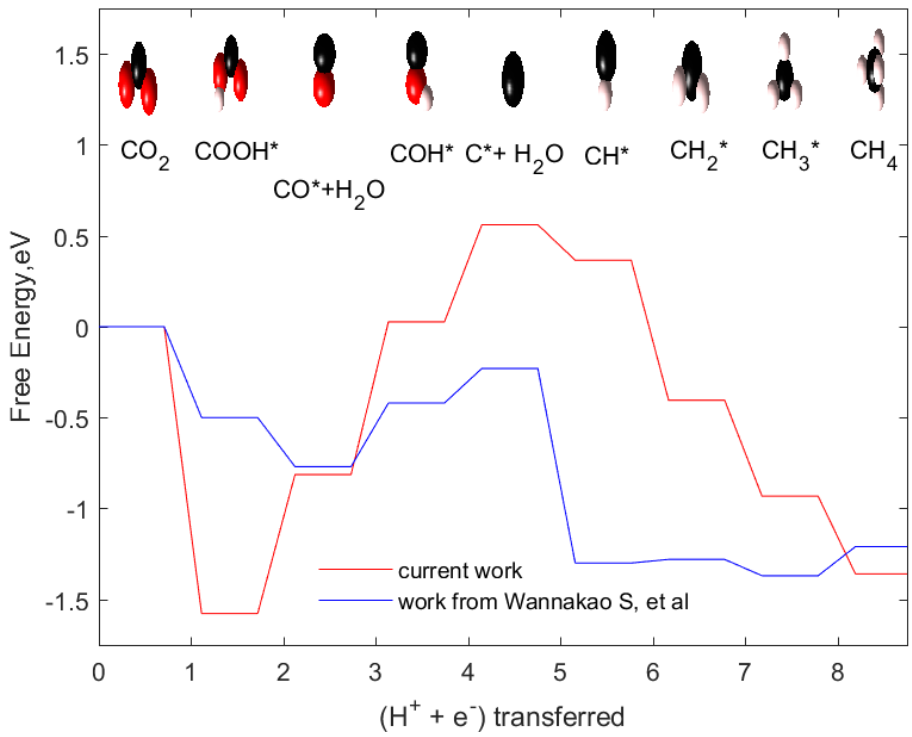

Figure 11. Lowest energy pathway for CO_2reduction to CH_4. Red: on graphene supported WC . Blue: on WC (0001) from the work of Wannakao S, et al. Color code of atoms: red: oxygen, black: carbon, white: hydrogen.

4. Conclusions

This work provides theoretical evidence that graphene supported WC nanoparticles could be a useful catalyst system for CO_2 reduction to light hydrocarbons and fuels. We have presented improved understanding of CO_2 reduction reaction mechanisms and provided the lowest energy pathway for various products. The results imply that CH_4 is favored over CH_3OH on this catalyst system because of the strong oxygen affinity towards WC. It is also worth noting that solvation effect plays an important role in determining the reaction pathway. We have shown how addition of solvation effect has shifted the rate-limiting step from CH_3OH formation step to COH* protonation step on the lowest energy pathway for CO_2 reduction to CH_3OH. At the same time, we have also shown how the binding free energies are overestimated in CH_4 reduction reaction when the effect of solvation is not considered thus resulting in higher limiting potentials. Addition of solvation effect to CH_4 reduction pathway has minimized the limiting potential by ~ 0.75V. On our catalyst system, CO_2 can reduce to CH_4 with an overpotential of 0.67V and to CH_3OH at higher negative potentials i.e. with an overpotential of 1.81V. We have also qualitatively compared results from current work with the work of Wannakao S et al. and explained the effect of adsorbate coverage in determining the energetics of CO_2 reduction reaction. Future work needs to focus on improving the efficiency of current catalyst system which can further minimize the reduction potential. This can be achieved by introducing catalytically active dopants, thereby tuning the electronic structure properties or by varying the WC nanoparticle size and interaction with the graphene support. Both of these routes are currently the subject of consideration for future work to build on the results from this manuscript.

Acknowledgments:

RBR gratefully acknowledges financial and research support from the Department of Chemical Engineering at Villanova University through his startup package fund. SA acknowledges financial support from the Department of Chemical Engineering and College of Engineering at Villanova University as well.

References

1. Hori, Y.; Kikuchi, K.; Suzuki, S. Production of CO and CH4 in electrochemical reduction of CO2 at metal electrodes in aqueous hydrogen carbonate solution. *Chemistry Letters*, *1985*, 1695–1698.
2. Kuhl, K.P.; Cave, E.R.; Abram, D.N.; Jaramillo, T.F. New insights into the electrochemical reduction of carbon dioxide on metallic copper surfaces. *Energy & Environmental Science*, *2012*, 7050–7059.
3. Selective electrochemical conversion of CO2 to C2 hydrocarbons. *Energy Conversion and Management*, *2010*, 30–32.
4. Opportunities and Challenges in Utilizing Metal-Modified Transition Metal Carbides as Low-Cost Electrocatalysts. *Joule*, *2017*, 253–263.
5. Platinum-like behavior of tungsten carbide in surface catalysis. science, 1973.
6. Zhong, Y.; Xia, X.; Shi, F.; Zhan, J.; Tu, J.; Fan, H.J. Transition metal carbides and nitrides in energy storage and conversion. *Advanced science*, *2016*, 1500286.
7. Liang, C.; Ying, P.; Li, C. Nanostructured β-Mo2C Prepared by Carbothermal Hydrogen Reduction on Ultrahigh Surface Area Carbon Material. *Chemistry of Materials*, *2002*, 3148–3151.
8. Michalsky, R.; Zhang, Y.J.; Medford, A.J.; Peterson, A.A. Departures from the Adsorption Energy Scaling Relations for Metal Carbide Catalysts. *The Journal of Physical Chemistry C*, *2014*, 13026–13034.
9. Wannakao, S.; Artrith, N.; Limtrakul, J.; Kolpak, A.M. Engineering Transition-Metal-Coated Tungsten Carbides for Efficient and Selective Electrochemical Reduction of CO2 to Methane. *ChemSusChem*, *2015*, 2745–2751.
10. Density functional theory study of iron and cobalt carbides for Fischer− Tropsch synthesis. *The Journal of Physical Chemistry C*, *2009*, 1085–1093.
11. Tungsten Carbides as Alternative Electrocatalysts: From Surface Science Studies to Fuel Cell Evaluation. *Industrial & Engineering Chemistry Research*, *2011*, 16–22.
12. Hunt, S.T.; Kokumai, T.M.; Zanchet, D.; Román-Leshkov, Y. Alloying tungsten carbide nanoparticles with tantalum: Impact on electrochemical oxidation resistance and hydrogen evolution activity. *The Journal of Physical Chemistry C* **2015**, *24*, 13691–13699.
13. Self-assembly of noble metal monolayers on transition metal carbide nanoparticle catalysts. *Science* **6288**, *2016*, 352–974.
14. The kinetics of the hydrogen oxidation reaction on WC/Pt catalyst with low content of Pt nanoparticles. *Journal of Electroanalytical Chemistry*, *2012*, 671–24.
15. A New Class of Electrocatalysts for Hydrogen Production from Water Electrolysis: Metal Monolayers Supported on Low-Cost Transition Metal Carbides. *Journal of the American Chemical Society*, *2012*, 3025–3033.
16. Catalytic Activity and Product Selectivity Trends for Carbon Dioxide Electroreduction on Transition Metal-Coated Tungsten Carbides. *The Journal of Physical Chemistry C*, *2017*, 20306–20314.
17. Thermal and electrochemical stability of tungsten carbide catalyst supports. *Journal of Power Sources*, *2007*, 431–440.
18. Metal carbides as alternative electrocatalyst supports. *Acs Catalysis*, *2013*, 1184–1194.
19. Wang, L.; Li, M.; Huang, Z.; Li, Y.; Qi, S.; Yi, C.; Yang, B. Ni–WC/C nanocluster catalysts for urea electrooxidation. *Journal of Power Sources*, *2014*, 264–282.
20. Antolini, E.. Graphene as a new carbon support for low-temperature fuel cell catalysts. *Applied Catalysis B: Environmental*, *2012*, 123–52.
21. Wannakao, S.; Artrith, N.; Limtrakul, J.; Kolpak, A.M. Engineering Transition-Metal-Coated Tungsten Carbides for Efficient and Selective Electrochemical Reduction of CO2 to Methane. *ChemSusChem*, *2015*, 2745–2751.
22. The relation of surface structure to the electrocatalytic activity of tungsten carbide. *Journal of Catalysis*, *1977*, 48–1.
23. MedeA®, M.. *Exploration and Design Analysis. Materials Design*; Inc, 2016.
24. Kresse, G.; Furthmüller, J. Software VASP, vienna. *Rev. B* **1996**, *54*, 169.
25. Hafner, J.. Ab-initio simulations of materials using VASP: Density-functional theory and beyond. *Journal of Computational Chemistry*, *2008*, 2044–2078.
26. Hafner, J.. Materials simulations using VASP—a quantum perspective to materials science. *Computer Physics Communications*, *2007*, 6–13.
27. Efficient iterative schemes for ab initio total-energy calculations using a plane-wave basis set. *Physical Review B* **1996**, *54*, 11169–11186.
28. The Vienna AB-Initio Simulation Program VASP: An Efficient and Versatile Tool for Studying the Structural, Dynamic, and Electronic Properties of Materials. In Properties of Complex Inorganic Solids; Boston, MA: US, 1997; pp. 69–82.

29. Improved Description of the Structure of Molecular and Layered Crystals: Ab Initio DFT Calculations with van der Waals Corrections. *The Journal of Physical Chemistry A*, *2010*, 11814–11824.
30. Theoretical Study of the Structural, Energetic, and Electronic Properties of 55-Atom Metal Nanoclusters: A DFT Investigation within van der Waals Corrections, Spin–Orbit Coupling, and PBE+U of 42 Metal Systems. *The Journal of Physical Chemistry C*, *2016*, 28844–28856.
31. Perspective: Advances and challenges in treating van der Waals dispersion forces in density functional theory. *The Journal of Chemical Physics*, *2012*, 120901.
32. π adsorption of ethene on to the {111} surface of copper: A periodic ab initio study of the effect of k-point sampling on the energy, atomic and electronic structure. *Surface Science*, *2000*, 93–103.
33. Peterson, A.A.; Abild-Pedersen, F.; Studt, F.; Rossmeisl, J.; Nørskov, J.K. How copper catalyzes the electroreduction of carbon dioxide into hydrocarbon fuels. *Energy & Environmental Science*, *2010*, 1311–1315.
34. Origin of the Overpotential for Oxygen Reduction at a Fuel-Cell Cathode. *The Journal of Physical Chemistry B*, *2004*, 17886–17892.
35. Theoretical Insight into the Trends that Guide the Electrochemical Reduction of Carbon Dioxide to Formic Acid. *ChemSusChem*, *2016*, 358–363.
36. Kuhl, K.P.; Hatsukade, T.; Cave, E.R.; Abram, D.N.; Kibsgaard, J.; Jaramillo, T.F. Electrocatalytic Conversion of Carbon Dioxide to Methane and Methanol on Transition Metal Surfaces. *Journal of the American Chemical Society*, *2014*, 14107–14113.
37. Hirunsit, P.. Electroreduction of Carbon Dioxide to Methane on Copper, Copper–Silver, and Copper–Gold Catalysts: A DFT Study. *The Journal of Physical Chemistry C*, *2013*, 8262–8268.
38. Implicit solvent models. Biophysical chemistry, 1999.
39. Implicit solvation models: equilibria, structure, spectra, and dynamics. Chemical Reviews, 1999.